

Electronic Supplementary Information (ESI)

Soluble, microporous, Tröger's Base copolyimides with tunable membrane performance for gas separation†

Yongbing Zhuang,^{‡ab} Jong Geun Seong,^{‡a} Yu Seong Do,^a Won Hee Lee,^a Moon Joo Lee,^c Zhaoliang Cui,^a Angel E. Lozano,^{de} Michael D. Guiver,^{*fga} and Young Moo Lee,^{*a}

^a *Department of Energy Engineering, College of Engineering, Hanyang University, Seoul 04763, Republic of Korea*
E-mail: ymlee@hanyang.ac.kr;

^b *College of Chemistry and Chemical Engineering, Hunan University of Arts and Science, Changde, Hunan, 415000, P. R. China*

^c *School of Chemical Engineering, College of Engineering, Hanyang University, Seoul 04763, Republic of Korea*

^d *Department of Macromolecular Chemistry, Institute of Polymer Science and Technology, ICTP-CSIC, 28006 Madrid, Spain*

^e *SMAP UA-UVA_CSIC, University of Valladolid, Valladolid, Spain*

^f *State Key Laboratory of Engines, School of Mechanical Engineering, Tianjin University, Tianjin 300072, P. R. China*
E-mail: michael.guiver@outlook.com;

^g *Collaborative Innovation Center of Chemical Science and Engineering (Tianjin), Tianjin 300072, P. R. China*

† Electronic Supplementary Information (ESI) available: Materials, synthetic details, characterization methods, analytical data as well as results from quantum chemical calculations using the Dmol3 module in Materials Studio 7.0. See DOI: 10.1039/c000000x/

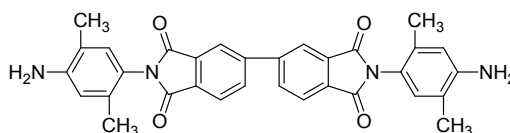
‡ Equally contributed to this work

1. Materials

We purchased dimethoxymethane (DMM, 99.0%), toluene (99.8%), and *N*-methyl-2-pyrrolidinone (NMP, >99.0%) from Sigma-Aldrich (Milwaukee, WI, USA) and used them as received. We obtained 3,3',4,4'-biphenyltetracarboxylic dianhydride (BPDA) and 4,4'-(9-fluorenylidene)dianiline (FDA) from Sigma-Aldrich and purified them by vacuum sublimation before use. We purchased 2,5-dimethyl-1,4-phenylenediamine (DPD), 4,4'-(9-fluorenylidene)di-*o*-toluidine (FDT), trifluoroacetic acid (TFA, >99%), and chloroform (>99.0%) from Tokyo Chemical Industry (TCI, Tokyo, Japan) and used them as received. We purchased ammonium hydroxide (25.0~25.8%) from Daejung Chemicals and Metals Co., Ltd. (Siheung, Gyeonggi-do, Korea). We synthesized the 9,9-spirobifluorene-2,2'-diamine (SBF) based on a previous report.¹

2. Synthesis and polymerization

2.1. Synthesis of An-BPDA

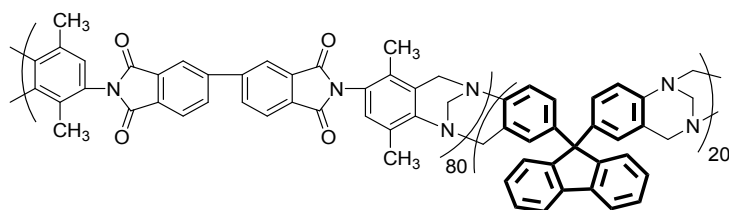


We synthesized the **An-BPDA** according to our previous reports,^{2,4} as shown in **Fig. 1**. In a four-necked flask, we dissolved DPD (8.1714 g, 60 mmol) in NMP (120 mL), and added FDA (5.8844 g, 20 mmol). After stirring it at room temperature for 12 h under nitrogen, we added 40 mL of toluene as an azeotropic agent and then heated the mixture to 180 °C for at least 9 h. While the toluene was refluxing, we removed the water with a Dean-Stark trap. We poured the resulting brownish solution into a mixture of water and methanol (2 L, V/V=1:1) under vigorous stirring. The resulting precipitate was filtered, washed with cold water (2 L), and dried to yield a yellow powder. We recrystallized the powder in ethanol twice and dried it at 80 °C in a vacuum oven before use. M_p (Melting point): 334.8 °C. Yield: 92.9%. ¹H NMR (300 MHz, DMSO-*d*₆): δ 1.94 (s, 6H), 2.04 (s, 6H), 5.09 (s, 4H), 6.57 (s, 2H), 6.85 (s, 2H), 8.05–8.07 (d, 2H), 8.35–8.37 (d, 2H), 8.38 (s, 2H). ¹³C NMR (300 MHz, DMSO-*d*₆): δ 167.3, 147.4, 144.5, 133.6, 132.7, 131.3, 130.1, 124.0, 122.2, 119.0, 118.5, 114.9, 17.2, 16.9. FTIR (powder, ν , cm⁻¹): 3467, 3391, 3229 (N-H stretching), 1773 (imide carbonyl symmetric stretching), 1716 (imide carbonyl asymmetric stretching), 1386 (imide -C-N). Anal. Calcd for C₃₂H₂₆N₄O₄: C, 72.44; H, 4.94; N, 10.56. Found: C, 71.79; H, 4.94; N, 10.62.

2.2. Synthesis of TB-based polyimides

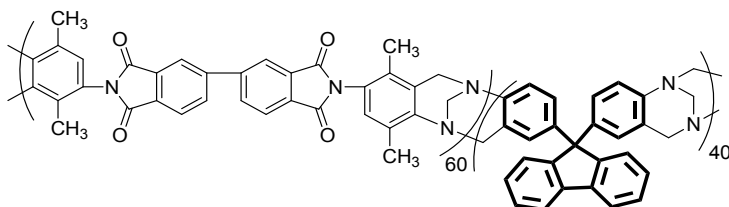
As shown in **Fig. 1**, we prepared **CoPI-TB-*x*** (*x*=1, 2, 3, 4, 5, and 6) by polymerizing DMM with **An-BPDA** and another fluorene-containing diamine from FDA, FDT, or SBF in TFA.^{2,3} Using **CoPI-TB-1** as an example, under nitrogen atmosphere, we dissolved **An-BPDA** (4.2416 g, 8.0 mmol) and FDA (0.6969 g, 2.0 mmol) in DMM (4.5 mL, 50.9 mmol) and cooled it in an ice bath. We added TFA (40 mL) dropwise over 10 min, stirred the mixture at room temperature for 48 h, and then carefully alkalized it with 2.5% aqueous ammonium hydroxide. We stirred the mixing solution to precipitate a white solid, which we filtered and washed three times with water and methanol. The product was purified by precipitation of a chloroform solution into methanol and dried at 120 °C for 24 h under vacuum to produce 4.75 g **CoPI-TB-1** powder (yield: 89.6%).

2.2.1. CoPI-TB-1



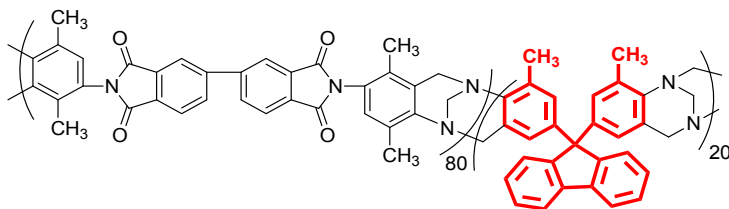
¹H NMR (300 MHz, CDCl₃): δ 1.94 (s, CH₃), 2.45 (s, CH₃), 3.91–4.53 (m, CH₂), 6.54–6.75 (t, H_{ar}), 6.95–7.05 (t, H_{ar}), 7.21–7.41 (m, H_{ar}), 7.74 (s, H_{ar}), 8.08 (s, H_{ar}), 8.24 (s, H_{ar}). ATR-FTIR (membrane, ν, cm⁻¹): 2952–2851 (C-H_x stretching), 1775 (imide carbonyl symmetric stretching), 1714 (imide carbonyl asymmetric stretching), 1374 (imide -C-N). Anal. Calcd for C_{33.6}H_{24.8}N_{3.6}O_{3.2}: C, 76.12; H, 4.71; N, 9.51. Found: C, 72.06; H, 4.62; N, 8.97. Molecular weight, by gel permeation chromatography, (NMP eluent, against polystyrene standards): $M_n = 68.8 \times 10^3$, $M_w = 190.9 \times 10^3$, PDI = 2.77. BET surface area = 61 m²/g, total pore volume = 0.12 cm³/g (at $p/p^0 = 0.98$, N₂ adsorption).

2.2.2. CoPI-TB-2



¹H NMR (300 MHz, CDCl₃): δ 1.94 (s, CH₃), 2.45 (s, CH₃), 3.91–4.53 (m, CH₂), 6.54–6.76 (t, H_{ar}), 6.95–7.05 (t, H_{ar}), 7.21–7.43 (m, H_{ar}), 7.74 (s, H_{ar}), 8.08 (s, H_{ar}), 8.24 (s, H_{ar}). ATR-FTIR (membrane, ν, cm⁻¹): 2946–2851 (C-H_x stretching), 1775 (imide carbonyl symmetric stretching), 1715 (imide carbonyl asymmetric stretching), 1374 (imide -C-N). Anal. Calcd for C_{32.2}H_{23.6}N_{3.2}O_{2.4}: C, 78.33; H, 4.82; N, 9.08. Found: C, 73.56; H, 4.54; N, 8.45. Molecular weight, by gel permeation chromatography, (NMP eluent, against polystyrene standards): $M_n = 59.5 \times 10^3$, $M_w = 174.6 \times 10^3$, PDI = 2.93. BET surface area = 401 m²/g, total pore volume = 0.40 cm³/g (at $p/p^0 = 0.98$, N₂ adsorption).

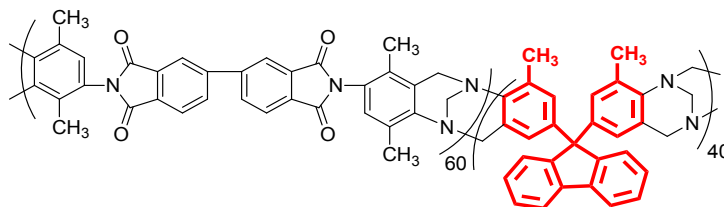
2.2.3. CoPI-TB-3



¹H NMR (300 MHz, CDCl₃): δ 1.94 (s, CH₃), 2.45 (s, CH₃), 4.03–4.53 (m, CH₂), 6.55 (br, s, H_{ar}), 6.93–7.05 (t, H_{ar}), 7.20–7.38 (m, H_{ar}), 7.73 (s, H_{ar}), 8.08 (s, H_{ar}), 8.24 (s, H_{ar}). ATR-FTIR (membrane, ν, cm⁻¹): 2961–2854 (C-H_x stretching), 1775 (imide carbonyl symmetric stretching), 1717 (imide carbonyl asymmetric stretching), 1374 (imide -C-N). Anal. Calcd for C₃₃H_{25.2}N_{3.2}O_{2.4}: C, 76.22; H, 4.82; N, 9.41. Found: C, 71.45; H, 4.82; N, 8.74. Molecular weight, by gel permeation chromatography, (NMP eluent, against polystyrene standards): $M_n =$

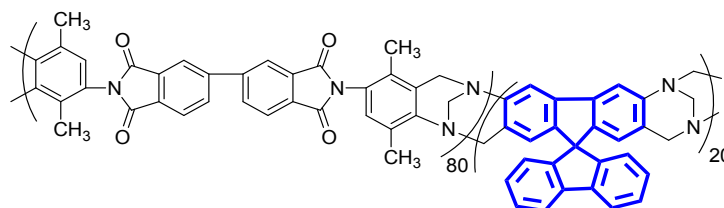
59.0×10^3 , $M_w = 171.6 \times 10^3$, PDI = 2.91. BET surface area = 154 m²/g, total pore volume = 0.13 cm³/g (at $p/p^0 = 0.98$, N₂ adsorption).

2.2.4. CoPI-TB-4



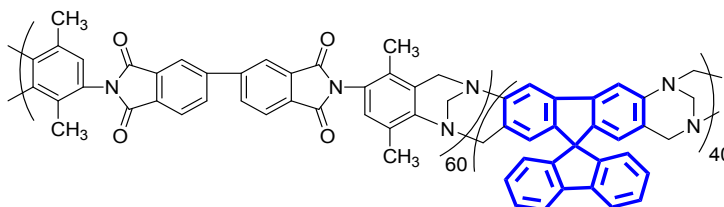
¹H NMR (300 MHz, CDCl₃): δ 1.94 (s, CH₃), 2.45 (s, CH₃), 3.90–4.73 (m, CH₂), 6.52 (br, s, H_{ar}), 6.94–7.05 (m, H_{ar}), 7.20–7.38 (m, H_{ar}), 7.73 (br, s, H_{ar}), 8.09 (s, H_{ar}), 8.25 (s, H_{ar}). ATR-FTIR (membrane, ν , cm⁻¹): 2961–2854 (C-H_x stretching), 1776 (imide carbonyl symmetric stretching), 1717 (imide carbonyl asymmetric stretching), 1374 (imide -C-N). Anal. Calcd for C₃₄H_{25.6}N_{3.6}O_{3.2}: C, 78.49; H, 5.03; N, 8.88. Found: C, 74.03; H, 5.00; N, 8.28. Molecular weight, by gel permeation chromatography, (NMP eluent, against polystyrene standards): $M_n = 58.7 \times 10^3$, $M_w = 171.9 \times 10^3$, PDI = 2.92. BET surface area = 277 m²/g, total pore volume = 0.34 cm³/g (at $p/p^0 = 0.98$, N₂ adsorption).

2.2.5. CoPI-TB-5



¹H NMR (300 MHz, CDCl₃): δ 1.94 (s, CH₃), 2.45 (s, CH₃), 3.87–4.74 (m, CH₂), 6.56–6.75 (m, H_{ar}), 6.93–7.05 (t, H_{ar}), 7.20 (s, H_{ar}), 7.30 (s, H_{ar}), 7.41 (s, H_{ar}), 7.72 (s, H_{ar}), 8.07 (br, s, H_{ar}), 8.23 (br, s, H_{ar}). ATR-FTIR (membrane, ν , cm⁻¹): 2962–2850 (C-H_x stretching), 1775 (imide carbonyl symmetric stretching), 1715 (imide carbonyl asymmetric stretching), 1374 (imide -C-N). Anal. Calcd for C_{33.6}H_{24.4}N_{3.6}O_{3.2}: C, 76.18; H, 4.64; N, 9.52. Found: C, 72.17; H, 4.70; N, 9.07. Molecular weight, by gel permeation chromatography, (NMP eluent, against polystyrene standards): $M_n = 51.5 \times 10^3$, $M_w = 150.6 \times 10^3$, PDI = 2.93. BET surface area = 181 m²/g, total pore volume = 0.30 cm³/g (at $p/p^0 = 0.98$, N₂ adsorption).

2.2.6. CoPI-TB-6



¹H NMR (300 MHz, CDCl₃): δ 1.94 (s, CH₃), 2.45 (s, CH₃), 3.87–4.74 (m, CH₂), 6.55–6.76 (m, H_{ar}), 6.96–7.05 (t, H_{ar}), 7.32 (s, H_{ar}), 7.40 (s, H_{ar}), 7.72 (s, H_{ar}), 8.06 (br, s, H_{ar}), 8.23 (br, s, H_{ar}). ATR-FTIR (membrane, ν , cm⁻¹):

2962–2851 (C-H_x stretching), 1776 (imide carbonyl symmetric stretching), 1717 (imide carbonyl asymmetric stretching), 1374 (imide -C-N). Anal. Calcd for C_{32.2}H_{22.8}N_{3.2}O_{2.4}: C, 78.46; H, 4.66; N, 9.09. Found: C, 74.21; H, 4.67; N, 8.72. Molecular weight, by gel permeation chromatography, (NMP eluent, against polystyrene standards): $M_n = 55.8 \times 10^3$, $M_w = 164.0 \times 10^3$, PDI = 2.93. BET surface area = 526 m²/g, total pore volume = 0.49 cm³/g (at $p/p^0 = 0.98$, N₂ adsorption).

3. Membrane fabrication

We prepared the membranes through solvent evaporation from 2–5 wt% polymer solutions in chloroform, as described previously.^{2,3} We filtered the solution with a 1.0- μ m filter cartridge to remove dust and poured it into a circular petri dish. The solvent evaporated slowly at room temperature and atmospheric pressure. After four days, we soaked the dry membranes in methanol overnight, then dried them at 120 °C under vacuum for more than 2 h and stored them at ambient pressure before testing.

4. Characterization methods

We measured nuclear magnetic resonance (NMR) with a Mercury Plus 300 MHz spectrometer (Varian, Palo Alto, CA, USA) using dimethyl sulfoxide-*d*₆ (DMSO-*d*₆) as a solvent. Both the Fourier transform infrared (FTIR) spectra of the diamine monomer powders and the attenuated total reflection mode FTIR (ATR-FTIR) spectra of the polymer membranes were measured using an infrared micro-spectrometer (IlluminatIR, SensIR Technologies, Danbury, CT, USA). Elemental analyses (EA) were performed with a ThermoFinnigan EA1108 (Fisons Instrument Co., Milan, Italy) elemental analyzer. Mechanical properties were tested with a Universal Testing Machine, UTM (AGS-J, Shimadzu, Kyoto, Japan) with specimens prepared according to ASTM D638-Type 5 recommendations. Molecular weight was measured by gel permeation chromatography (Waters GPC Systems, Milford, MA, USA) with polystyrene as an external standard and NMP as the eluent. Thermo-gravimetric analysis (TGA) was performed with a TGA Q50 instrument (TA Instrument, New Castle, DE, USA) at a heating rate of 10 °C/min under nitrogen. Differential scanning calorimetry (DSC) was performed on a TA Instruments Q20 calorimeter at a heating rate of 10 °C/min under nitrogen. The nitrogen adsorption/desorption behavior was measured at 77 K using a surface area and porosimetry analyzer (ASAP2020, Micrometrics Instrument Corp., Norcross, GA, USA) after degassing the samples at 150 °C at pressure lower than 10 μ mHg. Apparent surface areas were calculated from N₂ adsorption data by multi-point BET analysis. The densities were measured by a Sartorius LA 120S (Sartorius AG, Goettingen, Germany) balance with a density kit using the buoyancy method.² Fractional free volume (*FFV*, V_f) was calculated as follows:

$$V_{sp} = \frac{M_0}{\rho} \quad (1)$$

$$V_f = \frac{V_{sp} - 1.3 \times V_w}{V_{sp}} \quad (2)$$

where V_{sp} is the molar volume of polymer determined by the measured density, and V_w is the van der Waals molar volume based on Bondi's group contribution theory. Their densities were in the range of 1.175–1.215 g/cm³ at room temperature. Fractional free volume values estimated from the density measurements were within 0.186–0.207.

We tested gas permeation with a lab-made instrument using the time-lag method. We performed the test at 35 °C with a feed pressure of 1 bar. Downstream pressure in a fixed chamber volume increased from 0 to 10 mmHg against 760 mmHg of upstream pressure. Gas permeability coefficients were calculated from the slopes and intercepts in the steady-state pressure region as a function of time using the following equation:

$$P = \left(\frac{273.15 \cdot V \cdot l}{76 \cdot T \cdot \Delta p \cdot A} \right) \frac{dp}{dt} \quad (3)$$

where P (Barrer) is the gas permeability, T (K) is the measurement temperature, Δp (cmHg) is the pressure difference between upstream and downstream, l (cm) is membrane thickness, A (cm²) is the effective membrane area, and dp/dt is the rate of pressure increase in the downstream chamber at steady state. The ideal selectivity ($\alpha_{x/y}$) for components x and y was defined as the ratio of the gas permeability of the two components.

For mixed-gas permeation measurements, we determined the permeated gas concentrations by means of gas chromatography using a 490 Micro GC instrument (Agilent Technologies, Inc. Santa Clara, CA) equipped with a thermal conductivity detector. For CO₂/CH₄, the feed gas mixture was in a molar ratio of 1:1, and we measured the gas permeability as a function of CO₂ fugacity by the constant-pressure method at 35 °C.^{3, 5} Furthermore, to evaluate real hydrogen separation performances including H₂/N₂, H₂/CH₄, and H₂/CO₂ gas mixtures, experiments with binary mixtures of H₂ with another gas (N₂, CH₄, and CO₂, in a molar ratio of 1:1) were also conducted. In particular, to better understand the effect of aggressive CO₂ contents on the change of mixed-gas transport behaviors, the CO₂ fugacity dependence of mixed-gas permeabilities was investigated in a H₂/CO₂ molar ratio of 10:90, 30:70, 50:50, 70:30 and 10:90. The ratio of the permeate flow rate to the feed flow rate was set below 0.01 by controlling the sweep gas using a mass flow controller (Line Tech M3030VA), with a 10 cm³ (STP) min⁻¹ full scale. We measured the volumetric flow rate (cm³·min⁻¹) of gas in the permeate side using a bubble flow meter and determined the composition using a 490 Micro GC (Agilent Technologies, Inc. Santa Clara, CA USA) equipped with a thermal conductivity detector. Before each measurement, we conducted a calibration step, and we made at least three measurements to obtain an average of the permeate composition. The mixed gas permeability can be described as follows:

$$P = \frac{Q T_0 l}{T \Delta p A} \quad (4)$$

where Q (cm³·min⁻¹) is the gas flow rate, and all of the other abbreviations are the same as those in Equation (3). Therefore, the mixed gas CO₂/CH₄ selectivity, separation factor, can be obtained from

$$S_{F_{CO_2/CH_4}} = \frac{y_{CO_2}/y_{CH_4}}{x_{CO_2}/x_{CH_4}} \quad (5)$$

Here, x and y are the mole fractions in the feed and permeate side, respectively.

We obtained the energy barriers and the optimized configuration parameters (*e.g.*, dihedral angles in **Fig. 1**) using the conformers package and Dmol3 module, respectively, of Materials Studio 7.0. The select dihedral angles (bold and green-coded in **Fig. 1**) varied from -180° to $+180^\circ$ in the conformers package. The energy barriers (kcal/mol) to changes in the dihedral angles were calculated relative to the lowest energy attained ($\Delta E = E_i - E_{\min}$) over the 360° range. We performed the geometry optimizations for each conformer using a COMPASS force field and the Smart algorithm. Quantum chemical calculations for the repeat units were conducted by geometry optimization with the Dmol3 module to obtain the optimized configurations. All electron calculations were accomplished by the GGA/BLYP method with a DND basis set. The choice of integration accuracy and the orbital cutoff are medium.

5. Analyses and characterization

5.1. DSC analysis

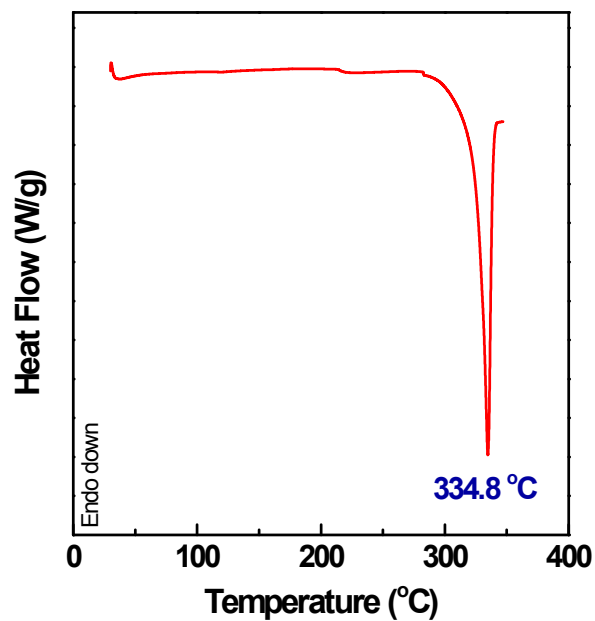


Fig. S1. DSC curve of the An-BPDA.

5.2. FTIR analysis

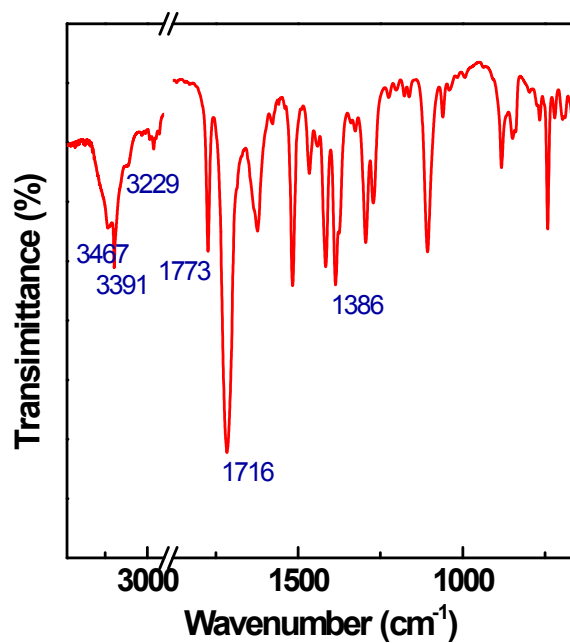


Fig. S2. FTIR of the An-BPDA.

5.3. ¹H NMR analysis

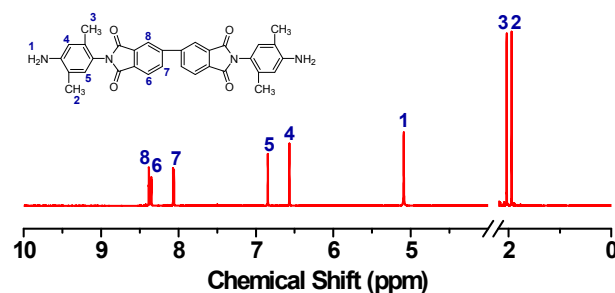


Fig. S3. ¹H NMR of the An-BPDA.

5.4. Nitrogen adsorption and desorption isotherms

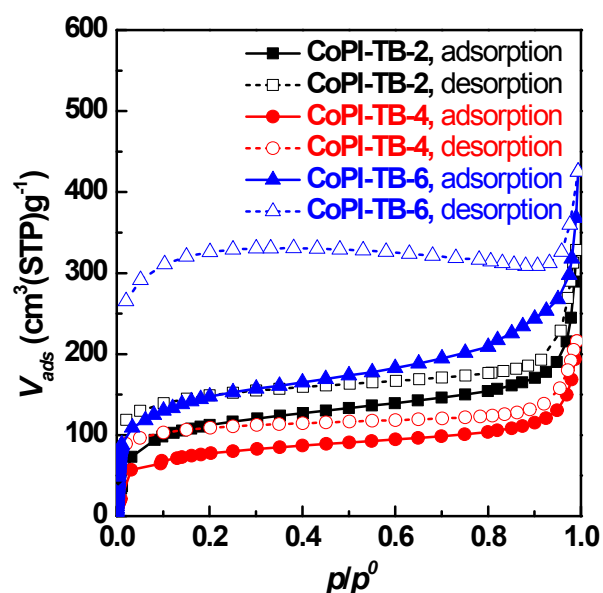


Fig. S4. Nitrogen adsorption (solid) and desorption (dash) isotherms at 77 K.

5.5. Solubility of the TB-based copolyimides

Table S1. Solubility of the TB-based copolyimides

polymer code	solvent							
	acetone	THF	DMSO	NMP	DMF	methanol	ethanol	chloroform
CoPI-TB-1	-	-	-	+	+	-	-	+
CoPI-TB-2	-	-	-	+	+	-	-	+
CoPI-TB-3	-	-	+-	+	+	-	-	+
CoPI-TB-4	-	+-	+	+	+	-	-	+
CoPI-TB-5	-	-	-	+	+	-	-	+
CoPI-TB-6	-	-	-	+	+	-	-	+

+, Soluble at room temperature; -, Insoluble at room temperature; +- Partially soluble at room temperature

5.6. Typical appearance of the CoPI-TB membranes

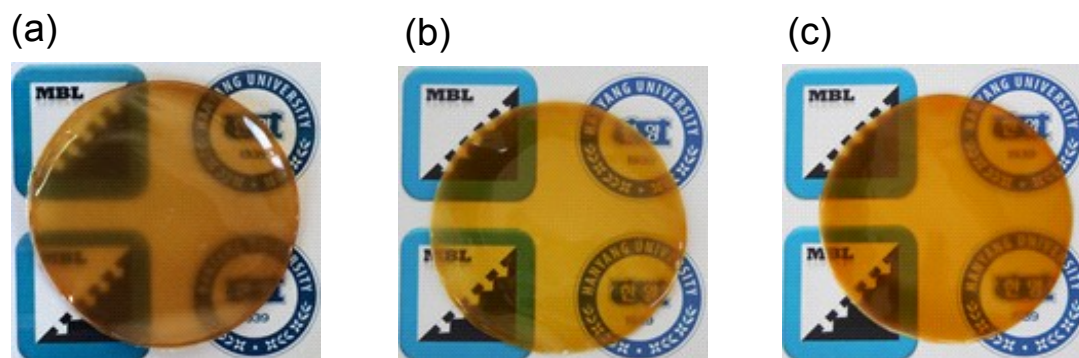


Fig. S5. The typical appearance of the representative membranes for (a) CoPI-TB-2, (b) CoPI-TB-4, (c) CoPI-TB-6.

5.7. TGA curves of the TB-based copolyimides

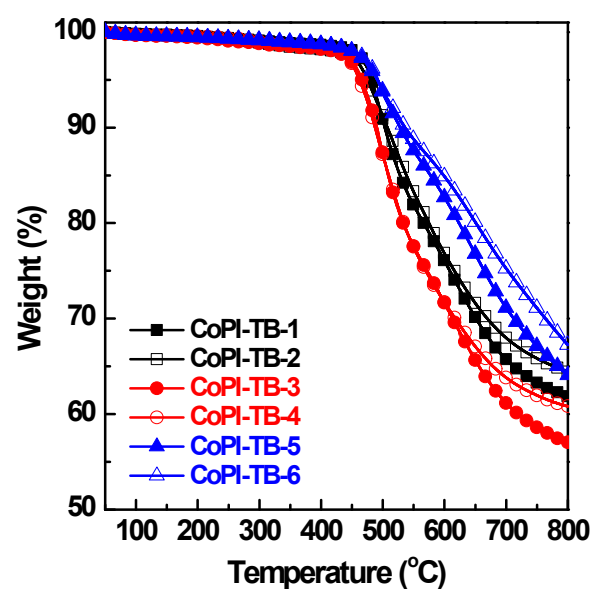


Fig. S6. TGA curves of the TB-based copolyimide membranes.

5.8. DMA curves of the TB-based copolyimides

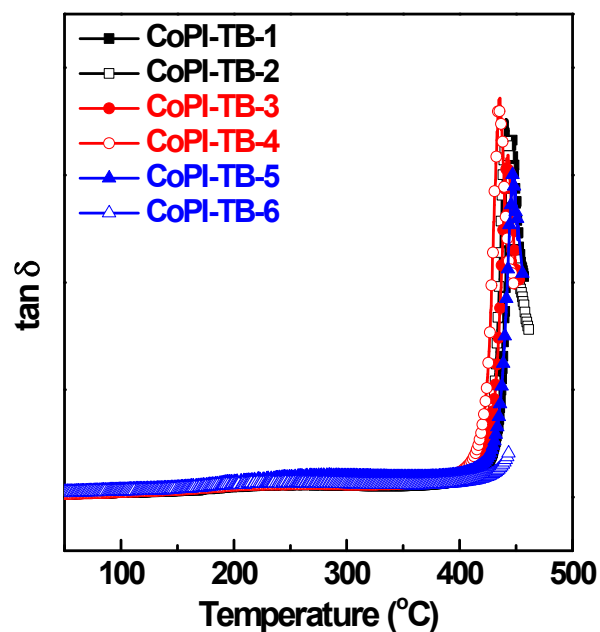


Fig. S7. DMA curves for the TB-based copolyimide membranes.

5.9. Mechanical properties of the TB-based copolyimides

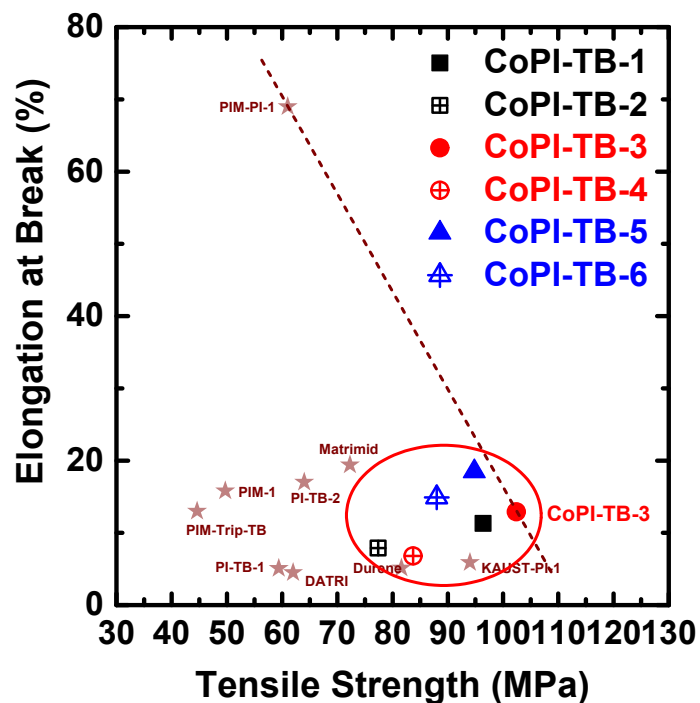


Fig. S8. A comparison of the mechanical properties of the TB-based copolyimides in this study, PIMs (PIM-1⁶ and PIM-Trip-TB⁷), PIM-PIs (PIM-PI-1⁸, KAUST-PI-1⁸, PI-TB-1 and PI-TB-2), high FFV PIs (6FDA-DATRI⁸ and 6FDA-Durene⁹), and commercial Matrimid[®].¹⁰ The dashed line indicates an arbitrary mechanical property tradeoff for polymers with high tensile strength or high elongation at break.

5.10. Pure gas transport properties (*P*, *D*, and *S*)**Table S2.** Single gas permeability (*P*), diffusivity (*D*), solubility (*S*), and ideal selectivity (α) for TB-based copolyimide membranes and reference polyimide membranes as a comparison

sample ^a		permeability (Barrer)						ideal selectivity (α) ^b				
		He	H ₂	N ₂	O ₂	CH ₄	CO ₂	H ₂ /N ₂	H ₂ /CH ₄	H ₂ /CO ₂	CO ₂ /CH ₄	CO ₂ /N ₂
CoPI-TB-1	<i>P</i>	139	249	7.0	34	7.0	158	36	36	1.6	23	23
	<i>D</i>	11759	3906	28	125	6.5	30	139.6	597.3	128	4.6	1.1
	<i>S</i>	0.09	0.5	1.9	2.1	8.2	40	0.26	0.06	0.01	4.8	21.1
CoPI-TB-2	<i>P</i>	230	403	10.2	53	10.1	209	39	40	1.9	21	21
	<i>D</i>	3267	4164	26	108	5.7	33	162.4	725.1	127	5.8	1.2
	<i>S</i>	0.54	0.7	3.0	3.8	13.3	48	0.24	0.06	0.02	3.6	16.0
CoPI-TB-3	<i>P</i>	223	371	9.5	47	8.9	196	39	42	1.9	22	21
	<i>D</i>	12798	4333	27	106	5.4	28	161.2	804.4	153	5.2	1.0
	<i>S</i>	0.13	0.7	2.7	3.3	12.6	53	0.24	0.05	0.01	4.2	19.6
CoPI-TB-4	<i>P</i>	362	667	19.9	96	17.9	241	34	37	2.8	13	12
	<i>D</i>	17837	8379	46	196	13	74	184	625.7	114	5.7	1.6
	<i>S</i>	0.15	0.6	3.3	3.7	10.2	25	0.18	0.06	0.02	2.5	7.5
CoPI-TB-5	<i>P</i>	177	334	10.4	48	11.4	228	32	29	1.5	20	22
	<i>D</i>	6080	4652	41	161	10	42	113.0	450.2	110	4.2	1.0
	<i>S</i>	0.22	0.5	1.9	2.3	8.4	41	0.28	0.07	0.01	4.9	21.6
CoPI-TB-6	<i>P</i>	243	472	16.4	73	19.0	330	29	25	1.4	17	20
	<i>D</i>	14026	5360	57	228	15	66	93.8	361.9	81	4.4	1.2
	<i>S</i>	0.13	0.7	2.2	2.4	9.8	38	0.31	0.07	0.02	3.9	17.3
CoPI-TB-1 ^c	<i>P</i>	110	202	6	26	5	110	33	37	1.8	20	18
	<i>D</i>	3931	3253	37	113	7.6	41	88	429	79	5.4	1.1
	<i>S</i>	0.21	0.5	1.3	1.8	5.5	20	0.37	0.09	0.02	3.7	16
CoPI-TB-2 ^c	<i>P</i>	155	291	8.1	38	7.6	154	36	39	1.9	20	19
	<i>D</i>	7183	4415	40	160	10	57	111	441	78	5.7	1.4
	<i>S</i>	0.16	0.5	1.6	1.8	5.7	21	0.31	0.09	0.02	3.6	13
Matrimid® 5218 ^{d,11}	<i>P</i>		27	0.28		0.21	7	97	129	3.9	33	25
	<i>D</i>		1740	4.13		0.93	8.97	421	1871	194	9.6	2.2
	<i>S</i>		0.1	0.5		1.7	5.9	0.2	0.06	0.02	3.5	12
6FDA-Durene ^{d,12}	<i>P</i>	358	585	39	135	34	678	15	17	0.9	20	17
	<i>D</i>					50	261				5.3	
	<i>S</i>					5	17				3.5	
KAUST-PI-1 ^{e,8}	<i>P</i>	1771	3983	107	627	105	2389	37	38	1.6 ⁿ	23	22
PIM-6FDA-OH ^{e,13}	<i>P</i>		259	11	45	9	263	24	29	1.0 ⁿ	29	24
6FDA-SBF ^{e,14}	<i>P</i>		234	7.8	35	6.4	182	30	37	1.3	28	23
6FDA-BSBF ^{e,14}	<i>P</i>		531	27	107	25	580	20	21	1.1 ⁿ	23	21
SBFDA-DMN ^{e,15}	<i>P</i>		2966	226	850	326	4700	13	9	1.6	14	21
6FDA-DATRI ¹⁶	<i>P</i>	198	257	8.1	39	6.2	189	32	42	1.4	31	23
PI-TB-1 ²	<i>P</i>	376	607	31	119	27	457	19	22	1.3	17	15
PIM-PI-1 ^{f,17}	<i>P</i>	260	530	47	150	77	1100	11	7	2.1 ⁿ	14	23
PIM-PI-3 ^{f,17}	<i>P</i>	190	360	23	85	27	520	16	13	1.4 ⁿ	19	23
PIM-PI-8 ^{f,17}	<i>P</i>	660	1600	160	545	260	3700	10	6	2.3 ⁿ	14	23
PIM-PI-10 ^{g,18}	<i>P</i>	300	670	84	270	168	2154	8.0	4	2.0 ⁿ	13	26
PIM-PI-12 ^{h,19}	<i>P</i>	1580	4230	369	1380	457	6340	12	9	1.5 ⁿ	14	17
BPDA-based polyimides												
BPDA-PI-BAFL ^{i,20}	<i>P</i>			0.61			23	38				38
BPDA-ODA ^{j,21}	<i>P</i>		5.2			0.03	0.87		173	6.0	29	
BPDA-MDA ^{j,21}	<i>P</i>		9.1			0.09	2.17		101	4.2	24	
BPDA-DDS ^{j,21}	<i>P</i>		11.3			0.09	2.57		126	4.4	29	
BPDA-DDBT ^{j,21}	<i>P</i>		31.2			0.24	8.2		130	3.8	34	
BPDA-DADM ^{k,22}	<i>P</i>	4.55		0.030	0.208	0.021	1.00				49	33
BPDA-DADS ^{k,22}	<i>P</i>	3.70		0.022		0.016	0.774				47	35
BPDA-PASN ^{k,22}	<i>P</i>	7.03		0.050	0.348	0.040	1.75				44	35
BPDA-HFIP ^{k,22}	<i>P</i>	34.2		0.757	3.79	0.460	16.8				37	22
BPDA-BAPE ^{k,22}	<i>P</i>	4.05		0.039	0.256	0.031	1.25				41	32
BPDA-BAPS ^{k,22}	<i>P</i>	6.01		0.054	0.368	0.040	1.85				47	34
BPDA-BAPP ^{k,22}	<i>P</i>	7.50		0.094	0.597	0.085	2.80				33	30

BPDA-HFBAPP ^{k,22}	<i>P</i>	18.3		0.305	1.67	0.216	7.33			34	24	
BPDA-MDT ^{k,22}	<i>P</i>	8.91		0.048	0.369	0.028	1.41			51	29	
BPDA-CDM ^{k,22}	<i>P</i>	6.92		0.031	0.260	0.016	0.978			60	32	
BPDA-MFA ^{k,22}	<i>P</i>	4.34		0.020	0.143	0.013	0.542			42	27	
BPDA-MCA ^{k,22}	<i>P</i>	3.67		0.011	0.096	0.006	0.335			61	31	
BPDA-MBA ^{k,22}	<i>P</i>	3.55		0.010	0.092	0.005	0.315			58	31	
BPDA-MDX ^{k,22}	<i>P</i>	31.8		0.913	4.73	0.818	22.40			27	25	
BPDA-HAB ^{k,22}	<i>P</i>	1.09		0.001	0.010	0.000	0.031			78	31	
BPDA-TSN ^{k,22}	<i>P</i>	12.0		0.076	0.577	0.037	2.74			74	36	
FDA-based polyimides												
PI-BAFL-BPDA ^{i,20}	<i>P</i>			0.61			23				38	
PI-BAFL-6FDA ^{i,20}	<i>P</i>			3.3			98				30	
CARDO ^{j,23}	<i>P</i>	166	4.5	24		164	37	1.0			36	
CARDO/ODA ^{j,23}	<i>P</i>	89	1.7	11		70	52	1.3			41	
HAB-FDA-6FDA (3:1) ^{m,24}	<i>P</i>			31		13	249			19	8	
HAB-FDA-6FDA (1:1) ^{m,24}	<i>P</i>			20		7.3	151			21	8	
HAB-FDA-6FDA (1:3) ^{m,24}	<i>P</i>			13		4.7	100			21	8	
FDA-HFBAPP-BPDA ^{f,25}	<i>P</i>	31.4	33.6	0.65	3.46	0.50	18.2	52	67	1.8	36	28
FDA-HFBAPP-BTDA ^{f,25}	<i>P</i>	17.5	16.2	0.22	1.40	0.17	7.0	74	95	2.3	41	32
FDA-HFBAPP-6FDA ^{f,25}	<i>P</i>	72.5	71.4	1.99	9.34	1.28	46.5	36	56	1.5	36	23

^a Units: *P*: 10⁻¹⁰cm³(STP)/cm sec cmHg, *D*:10⁻⁹cm²/sec, and *S*: cm³(STP)/cm³ atm, measured at 1 atm, 35 °C;

^b Ideal selectivity $\alpha=P_1/P_2$;

^c measured at 3 bar, 35 °C;

^d measured at 3.5 atm, 35 °C;

^e measured at 2 bar, 35 °C;

^f measured at 1 bar, 30 °C;

^g measured at 1 bar, room temperature (20-22 °C);

^h measured at 1 bar, 25 °C;

ⁱ measured at 1 atm, 25 °C;

^j measured at 10 atm, 50 °C;

^k measured at 1.5 bar, 35 °C;

^l measured at 3 bar, 20 °C;

^m measured at 10 bar, 35 °C;

ⁿ CO₂/H₂.

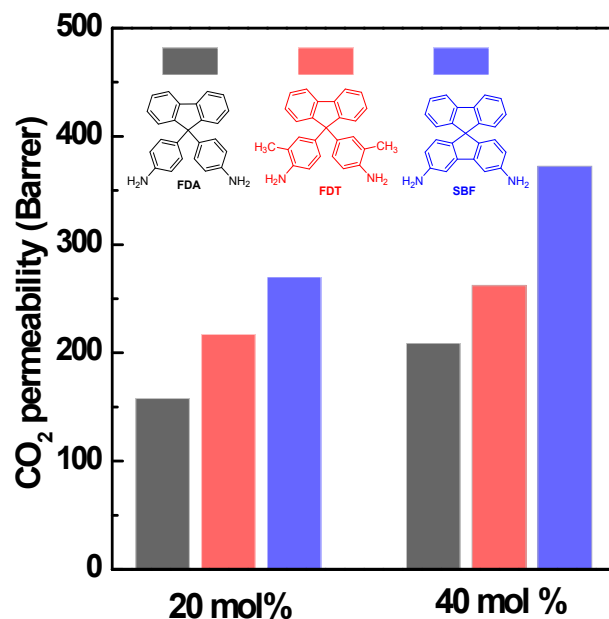
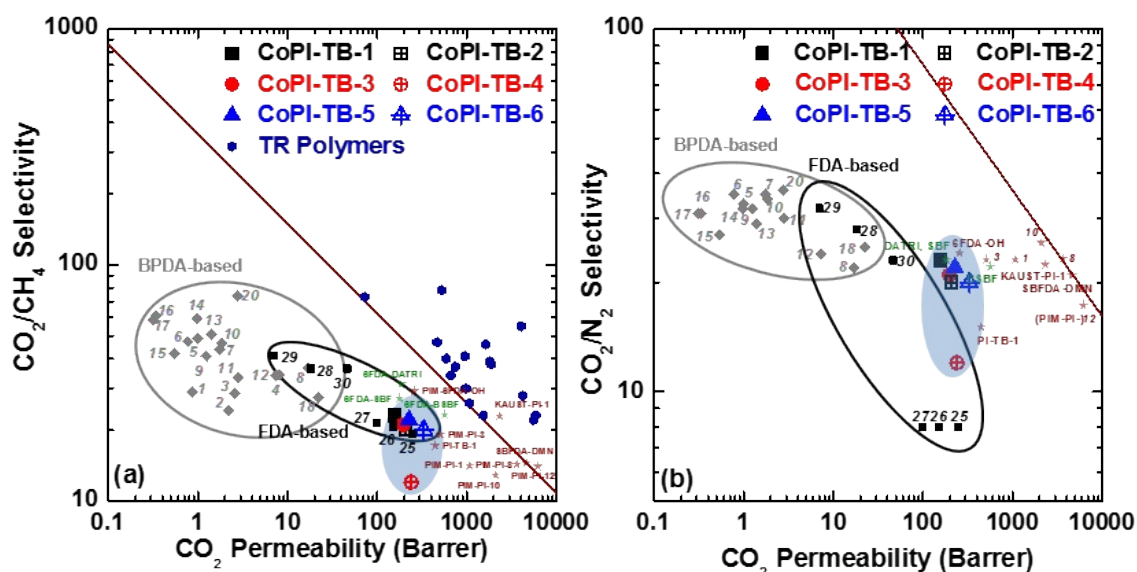
5.11. Variation of CO₂ transport behaviors of the TB-based copolyimidesFig. S9. Variation of CO₂ permeability with fluorene-containing diamine contents of the copolyimides.

Fig. S10. Robeson plot relevant to TB-based copolyimide membranes for (a) CO₂/CH₄ and (b) CO₂/N₂ (solid lines represent the 2008 upper bound). Data from reported Thermally rearranged (TR) polymers (navy-colored), PIM-PIs (wine), high free-volume polyimides (olive), BPDA-based (grey), and FDA-based polyimides (black) are included for comparison. 1, BPDA-ODA; 2, BPDA-MDA; 3, BPDA-DDS; 4, BPDA-DDBT; 5, BPDA-DADM; 6, BPDA-DADS; 7, BPDA-PASN; 8, BPDA-HFIP; 9, BPDA-BAPE; 10, BPDA-BAPS; 11, BPDA-BAPP; 12, BPDA-HFBAPP; 13, BPDA-MDT; 14, BPDA-CDM; 15, BPDA-MFA; 16, BPDA-MCA; 17, BPDA-MBA; 18, BPDA-MDX; 19, BPDA-HAB; 20, BPDA-TSN; 21, PI-BAFL-BPDA; 22, PI-BAFL-6FDA; 23, CARDO; 24, CARDO/ODA; 25, HAB-FDA-6FDA (3:1); 26, HAB-FDA-6FDA (1:1); 27, HAB-FDA-6FDA (1:3); 28, FDA-HFBAPP-BPDA; 29, FDA-HFBAPP-BTDA; and 30, FDA-HFBAPP-6FDA; Data are shown in **Table S2** and data relevant to TR polymers.²⁶

For the case of CO₂/CH₄ separations, the TB-based copolyimides also show good plasticization resistance (Fig. 3) although their pure gas separation performances are located below the 2008 upper bounds (Fig. S10 (a), see ESI). However, for the CO₂/N₂ separation, they were situated farther away from the bound, indicating that they exhibited relatively lower performance than for the other gas pairs (Fig. S10 (b), ESI). Note that there is an apparent limit of the enhancement in CO₂

separation performances even after architecturing BPDA-based polyimides with fluorene diamines and TB units. However, Fig. S10 also reveals that high *FFV* polyimides bearing 6FDA moieties (olive) and PIM-PI copolymers (wine) also appear to exhibit a limit, lying below the 2008 Robeson upper bounds, whereas CO₂/CH₄ separations for all the Thermally rearranged (TR) polymers presented excellent performance surpassing the upper bound. An improvement in CO₂ solubility of CoPI-TB membranes occurs by introducing tertiary amines in the TB units, which interact with CO₂ molecules.²⁻⁴ The CO₂ solubility enhancement promotes CO₂/CH₄ and CO₂/N₂ sorption selectivities, which results preferentially in sorption selectivity over diffusion selectivity. As listed in Table S2, all of TB-based copolymers in this study show comparable or even greater sorption selectivities for the CO₂/CH₄ and CO₂/N₂ separations rather than diffusion selectivity, which is similar to PIM-PIs but totally different from TR polymers.^{27, 28} Therefore, CoPI-TB membranes can fulfill an important role for complementary gas separation applications, where TR polymers encounter challenges for separations such as H₂/N₂, H₂/CH₄ and H₂/CO₂.

5.12. Variation of H₂ transport behaviors of the TB-based copolyimides

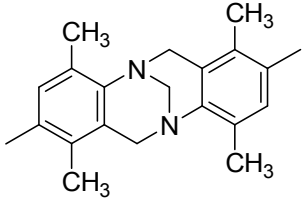
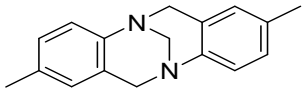
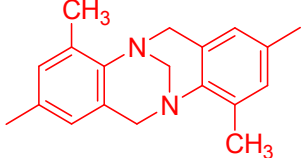
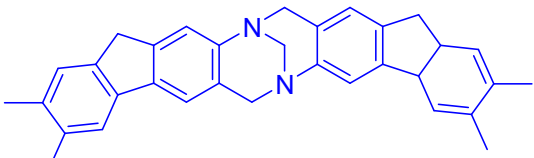
All TB-based copolyimides except **CoPI-TB-4** show single gas separation performances below the Robeson upper bounds for H₂/CH₄ and H₂/N₂ separation. However, as shown in the Fig. 2 and Table S2, there have been few reports on solely polymeric membrane materials (i.e. without additional post-treatment and/or mixing with inorganic materials) with the excellent hydrogen gas separation performances except for PIM-PI-12,¹⁹ SBFDA-DMN,¹⁵ and KAUST-PI-1.⁸ Even compared to the aforementioned PIM-PI membranes or 6FDA-based PI membranes, which are well known as the one of the most highly permeable membranes ever reported, the TB-based copolyimides in this study present comparable or enhanced hydrogen gas separation performances. For example, **CoPI-TB-6** membranes, which had the lowest hydrogen separation performances in this study, for H₂/CH₄ and H₂/N₂ is nearly 3.5 and 2.6 times higher, respectively, than those for PIM-PI-1.

Furthermore, from a molecular architecture point of view, the TB-based copolyimides in this study are amenable to allow tailoring of gas separation performances by using only commercially available monomers and a relatively facile synthetic method, different from PIMs. Especially, BPDA-based polyimides are known to present generally lower gas permeability because of their non-contorted chain configurations, which result in low free-volume in the membranes. Thus, there have been few reports on BPDA-based PIs as membrane materials at a commercial level for gas separation except for Upilex-R[®], BPDA-ODA polyimide membranes, despite their excellent thermal and mechanical properties. Therefore, until now, there have been no reported PIMs or PIM-PIs incorporating BPDA units. Note that all of the CoPI-TB membranes incorporating BPDA as a dianhydride in this study exhibit an unprecedented improvement in hydrogen permeability by about two orders of magnitude compared to BPDA-based polyimides (for instance, **CoPI-TB-6** (472 Barrer) and Upilex-R[®], BPDA-ODA (5.2 Barrer) as shown in the Fig. 2 and Table S2, while maintaining reasonably good hydrogen/gas selectivities. The present CoPI-TB membranes containing BPDA units are located much closer to the Robeson upper bound. This improvement results from incorporating stiff and bulky moieties from the fluorene-based diamines, FDA, FDT, and SBF. These diamines inhibit effective interchain packing and reduce the rotational mobility of the main chains to enhance gas transport performance.

In comparison with FDA-based polyimides as shown in Fig. 2 and Table S2, for example, **CoPI-TB-1** and **CoPI-TB-2** membranes bearing FDA moieties still present enhanced hydrogen separation performances. In the case of (FDA:HFBAPP, 1:1)-BPDA (**28**) copolyimide membranes, although they contained the same amount of BPDA and 30 mol% larger amount of FDA units, the H₂ permeability of (FDA:HFBAPP, 1:1)-BPDA (34 Barrer) was 7.4 times smaller than **CoPI-TB-1** (249 Barrer). The permeability difference arises from the introduction of the V-shaped stiff TB units. Such subtle structural adjustments in the copolyimide backbones would be expected to further restrict effective interchain packing and thus enhance gas transport in the membranes. PI-BAFL-BPDA (**21**) membranes are also good examples to demonstrate this TB effect. The CO₂ permeability of **CoPI-TB-1** and **CoPI-TB-2** is about 7-fold and 9-fold, respectively, higher than that of the previous PI-BAFL-BPDA (*P*(CO₂) = 23 Barrer) derived from the same monomers, BPDA and FDA, because of the additional free volume imparted by the V-shaped TB units in improving permeability. Combined with the functionality of these fluorene-containing bulky diamines and rigid TB groups in the backbones, the resulting CoPI-TB membranes containing BPDA as a dianhydride introduce an obvious enhancement in the hydrogen separation performances.

5.13. Molecular models of TB-based units in backbones

Table S3. Comparison of van der Waals volume (V_w) values of V-shaped TB scaffolds in different copolymer backbones.

copolymer	V-shaped TB block	V_w (cm^3/mol)
TB-DPD		156.23
TB-FDA		116.76
TB-FDT		136.60
TB-SBF		203.12

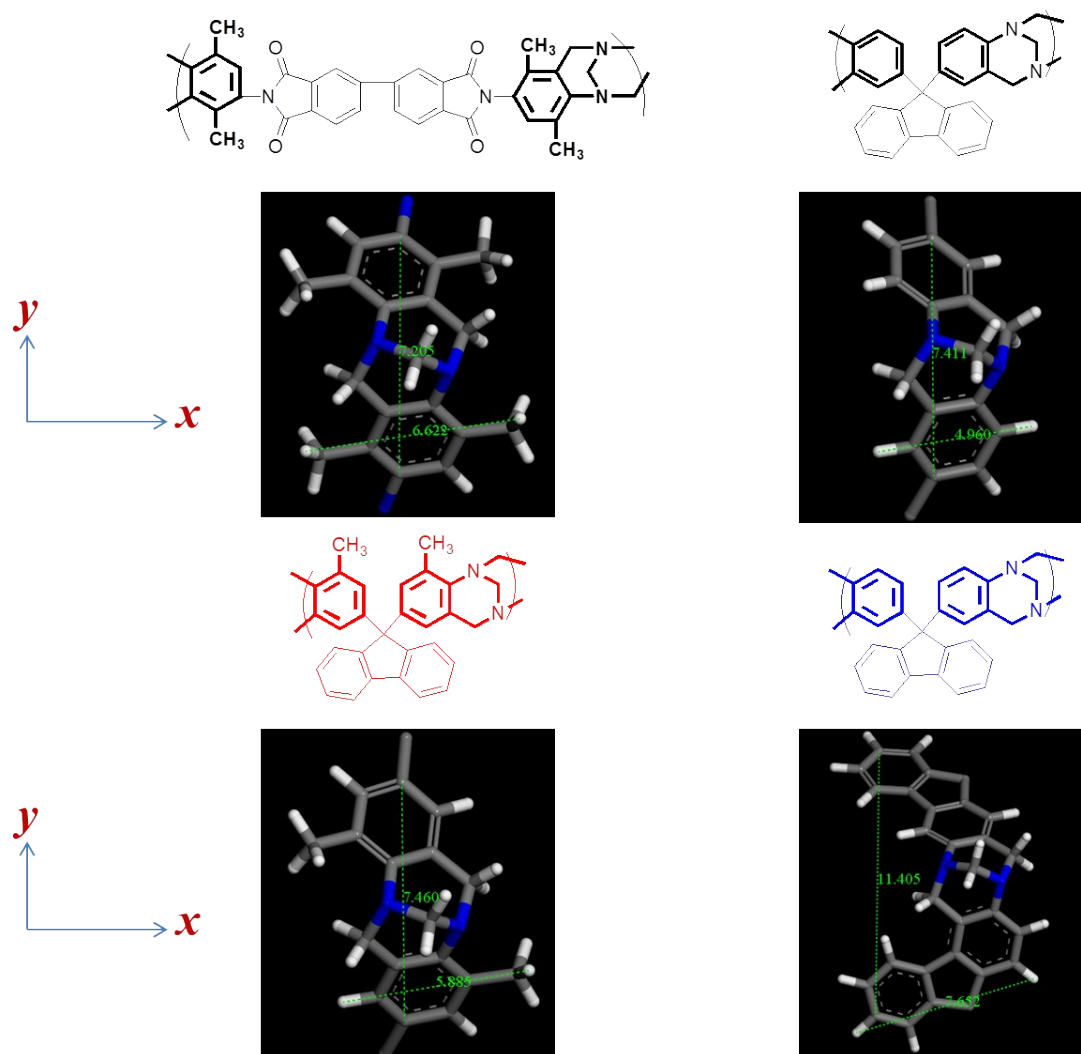


Fig. S11. Three-dimensional molecular models for V-shaped TB scaffolds (TB-FDA, TB-FDT, and TB-SBF) relative to TB units in copolyimide backbones from quantum chemical calculations using the Dmol3 module in Materials Studio 7.0. DPD-base V-shaped TB scaffold (TB-DPD) as comparison.

Table S4. Projection distances between two terminal carbon atoms along x axis and those between two terminal hydrogen atoms along y axis for FDA-based, FDT-based, and SBF-based V-shaped TB scaffolds (TB-FDA, TB-FDT, and TB-SBF) relative to TB units in copolyimide backbones from quantum chemical calculations using the Dmol3 module in Materials Studio 7.0. DPD-base V-shaped TB scaffold (TB-DPD) as comparison

copolymer	x axis (pm)	y axis (pm)
TB-DPD	662.2	720.5
TB-FDA	496.0	741.1
TB-FDA	588.5	746.0
TB-SBF	765.2	1140.5

5.14. Mixed-gas separation performances

5.14.1. H₂ mixed-gas separation performances

Table S5. H₂ pure and mixed gas separation performances for selected CoPI-TB-1 and CoPI-TB-2 membranes and reference polyimide membranes as a comparison

sample		pure gas separation			mixed-gas separation		
		$P_{H_2}^a$	P_X^a	$\alpha_{H_2/X}^c$	$P_{H_2}^{*b}$	P_X^{*b}	$S_{F,H_2/X}^d$
CoPI-TB-1	$X=N_2$	202	6	33	70	2.1	33
	$X=CO_2$		110	1.8	63 ^e	75 ^e	0.8
					46 ^f	40 ^f	1.2
					28	37	0.8
					11 ^g	35 ^g	0.3
			2 ^h	29 ^h	0.1		
CoPI-TB-2	$X=N_2$	291	8.1	36	147	4.4	33
	$X=CH_4$		7.6	39	159	5.6	28
	$X=CO_2$		154	1.9	205 ^e	238 ^e	0.9
					150 ^f	179 ^f	0.9
				81	143	0.6	
				41 ^g	107 ^g	0.4	
				19 ^h	132 ^h	0.1	
Matrimid 5218 ²⁹	$X=N_2$	24 ⁱ	0.17 ⁱ	139	24 ^j	N/V	N/V
	$X=CO_2$		5.6 ⁱ	4.2	16 ^k	5.7 ^k	2.8 ^l
6FDA-Durene ³⁰	$X=CO_2$	600 ^m	581 ^m	1.0	194 ⁿ	586 ⁿ	0.3 ^l

^a P , pure gas permeability ($10^{-10} \text{cm}^3(\text{STP})/\text{cm sec cmHg}$ (Barrer)), measured at 3 bar, 35 °C, constant volume method (Timelag method);

^b P^* , mixed-gas (50:50 H₂/X mixture, total feed pressure of 6 bar) permeability ($10^{-10} \text{cm}^3(\text{STP})/\text{cm sec cmHg}$ (Barrer)), measured at H₂ fugacity of 3 bar, 35 °C, constant pressure method;

^c Ideal selectivity, $\alpha = P_1/P_2$;

^d Separation Factor, $S_F = (y_1/y_2)/(x_1/x_2)$, x and y are the mole fractions in the feed and permeate side, respectively;

^e mixed-gas (90:10 H₂/CO₂ mixture, total feed pressure of 6 bar);

^f mixed-gas (70:30 H₂/CO₂ mixture, total feed pressure of 6 bar);

^g mixed-gas (30:70 H₂/CO₂ mixture, total feed pressure of 6 bar);

^h mixed-gas (10:90 H₂/CO₂ mixture, total feed pressure of 6 bar);

ⁱ measured at 4 bar, 30 °C;

^j mixed-gas (50:50 H₂/N₂ mixture, total feed pressure of 4 bar, 30 °C), There showed no information on the N₂ mixed-gas permeability and the relevant separation factor, however, it was written in the literature that "H₂ transport is not affected by the presence of N₂ as co-partner in the overall gas transport.";

^k measured at 30 °C;

^l Mixed-gas selectivity, $\alpha^* = P_1^*/P_2^*$;

^m measured at 3.5 atm, 35 °C;

ⁿ mixed-gas (50:50 H₂/CO₂ mixture, total feed pressure of 7 atm)

Table S5 presents H₂ pure and mixed gas separation performances for CoPI-TB-1 and CoPI-TB-2 membranes. Compared to the pure hydrogen gas permeability at H₂ feed pressure of 3 bar (291 Barrer) with CoPI-TB-2 membranes, for example, all of hydrogen gas permeabilities from the mixtures decreased from 45% (CH₄, 159 Barrer) to 72% (CO₂, 81 Barrer) (Table S2 and S5). These findings correspond well with the cases of Matrimid® 5218 and 6FDA-Durene membranes.^{29, 30} For example, pure H₂ gas permeability for 6FDA-Durene membranes was 600 Barrer and it declined by 68% to 194 Barrer at the 50:50 H₂/CO₂ mixture, which was comparable to the case of CoPI-TB-1 and CoPI-TB-2 membranes. Interestingly, different from hydrogen permeabilities aforementioned, there was no decline or a slight decline in the mixed gas permeabilities of the other gases including N₂, CH₄, and CO₂ for CoPI-TB-2 as well as reference polymer membranes. In the case of mixed-gas separation for CoPI-TB-2 membranes, N₂, CH₄, and CO₂ permeabilities decreased by 46%, 26%, and 7%, respectively. It is apparent that the gases with larger solubility, such as CH₄, and CO₂, show a more negligible change in the mixed-gas permeability compared with the pure gas permeability than the gas with smaller solubility such as N₂, resulting in a rapid drop in the H₂/corresponding gas separation factor as listed in Table S5. For the H₂/N₂ (N₂: low solubility) mixed-gas separation for CoPI-TB-2 membranes, only a small decrease of about 8% in the permeability was observed, from 36 Barrer (pure gas) to 33 Barrer (mixed-gas). On the other hand, H₂/CO₂ (CO₂: large solubility) mixed-gas separation factor of the same membrane showed a distinct decline, 68% (from 1.9 Barrer for pure gas to 0.6 Barrer for mixed gas). These results indicate differences in the competitive sorption between H₂-N₂ and H₂-CO₂. CO₂ solubility at a feed pressure of 3 bar for CoPI-TB-2 membranes was 21 cm³(STP)/cm³ atm, 42-fold larger than H₂ (0.5 cm³(STP)/cm³ atm) and 13-fold larger than N₂ (0.5 cm³(STP)/cm³ atm) (Table S2). Furthermore, H₂/CO₂ sorption selectivity for CoPI-TB-2 membranes was 0.02 and H₂/N₂ was

0.31, meaning that there is a 13 times larger competition when H₂ and CO₂ molecules were absorbed into the **CoPI-TB-2** membrane compared with that of H₂ and N₂. The pronounced CO₂ sorption and subsequent drop in H₂/CO₂ separation performances in the H₂-CO₂ mixtures was also observed in the Matrimid® 5218 and 6FDA-Durene membranes.^{29, 30}

To better understand the effect of CO₂ contents on the change of mixed-gas transport behaviors, the CO₂ fugacity dependence of mixed-gas permeabilities was also investigated at a H₂/CO₂ molar ratio of 10:90, 30:70, 50:50, 70:30 and 10:90. For **CoPI-TB-2** membranes, both H₂ and CO₂ mixed gas permeabilities steadily decreased with increasing CO₂ molar ratios up to 90%. However, the permeability decrement in H₂ was more dramatic than CO₂ (Table S5). Even CO₂ mixed gas permeabilities at low CO₂ molar ratios (10% and 30%) were larger than pure CO₂ gas permeability. These results indicate that larger CO₂ sorption affinity and thereafter better interaction with the TB-based copolymer membranes in this study would impede hydrogen molecules in mixtures from permeating through the membranes and this trend is more unambiguous with increasing CO₂ molar ratios. Therefore, hydrogen mixed-gas separation performances would be reduced. 6FDA-Durene polyimide membranes are also a representative example to demonstrate these phenomena.¹² At a 50 mol% aggressive CO₂ content in the mixture, H₂/CO₂ mixed-gas selectivity for 6FDA-Durene membranes showed a significant 70% drop to 0.3 while CO₂ mixed gas permeability (586 Barrer) was similar to pure CO₂ gas permeability (581 Barrer).

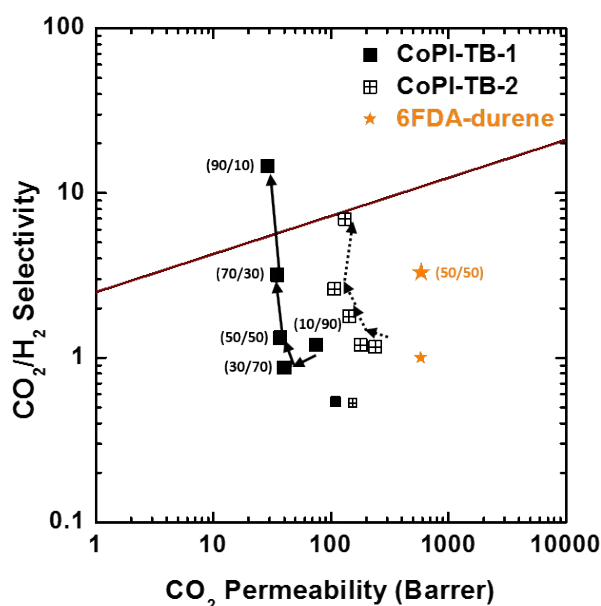


Fig. S12. Robeson plot relevant to CoPI-TB-1 and CoPI-TB-2 membranes for pure and mixed-gas CO₂/H₂ separation performances (solid lines represent the 2008 upper bound) with the arrows indicating the increase in CO₂ molar ratio from 10% to 90%. Values for CO₂/H₂ molar ratio are given between parentheses. Data from reported 6FDA-Durene (orange, star-shaped) are included for comparison. Smaller points are pure gas feeds at 3 bar and larger ones are mixed-gas at feed pressure 6 bar. Data are shown in **Table S5**.

Surprisingly, FDA-based CoPI-TB membranes (**CoPI-TB-1** and **CoPI-TB-2**) show CO₂-reverse selective characteristics with increasing CO₂ molar ratios as shown in Fig. S12.³¹⁻³⁴ While the Robeson upper bound plots are intended solely for pure gas permeabilities in polymer membranes, it is instructive to also benchmark mixed gas data to assess the trend as a function of CO₂ molar ratios, which are more relevant to industrial application. Similar to the 6FDA-Durene polyimides, CO₂/H₂ separation performances for FDA-based CoPI-TB membranes were enhanced with an increase in the CO₂ molar ratio. Especially, the CO₂/H₂ separation factor for **CoPI-TB-1** at a CO₂ molar ratio of 90% was above the Robeson upper bound. Therefore TB-based copolyimide membranes have a potential for membrane gas separation of H₂ and CO₂ binary mixtures.

5.14.2. CO₂ mixed-gas separation performances and plasticization responses in copolyimides

Compared to pure CO₂ permeability (Table 2 and Table S2), CO₂ permeability at low CO₂ fugacity (< 3 bar) in CO₂/CH₄ (50/50) binary mixtures for all TB-based copolyimides were retained or slightly decreased. For example, pure CO₂ permeability at 1 bar of **CoPI-TB-1** was 158 Barrer, and CO₂ permeability in the binary mixture at 3 bar was 140 Barrer. We found an initial decline of CO₂ permeability with increasing CO₂ fugacity for all TB-based copolyimides in the mixed gas (Fig. 3(a)) because of reductions in the solubility coefficient of CO₂ with increasing feed pressure, following the dual-mode sorption model.³⁵ As the CO₂ fugacity surpassed 10 bar, the TB-based copolyimides maintained an almost constant CO₂ permeability. This trend differs from that of a recently reported semi-ladder PIM-PI, the 'unannealed' (heated at 120 °C for 24 h under vacuum without further thermal annealing) TPDA-APAF (UA-TPDA-APAF) membrane,³⁶ which showed an obvious up-turn of CO₂ permeability above 10 bar (Fig. 3(a)), indicative of CO₂-induced plasticization (*c.f.* UA-TPDA-APAF membranes surprisingly showed a plasticization resistance after thermal annealing at 250 °C for 24 h, indicating that with increasing CO₂ fugacity up to 20 bar, no up-turn in mixed gas CH₄ permeability and thereafter no deterioration of CO₂/CH₄ separation factor occurred compared to the CO₂/CH₄ ideal gas selectivity). PIM-6FDA-OH¹³ showed a subtle uptick of CO₂ permeability, from 163 Barrer at 12.5 bar (minimum) to 172 Barrer at 21.0 bar (see Table S3 in the Supplementary Information Section of Ref. 13). A more persuasive indicator of plasticization would be the mixed-gas permeability of slower CH₄ gas. The moderately permeable copolyimides, **CoPI-TB-x** ($x = 1-5$), exhibited almost constant CH₄ permeability up to a CO₂ fugacity of 17 bar (Fig. 3(b)), similar to cross-linked thermally rearranged poly(benzoxazole-co-imide) membranes,³⁷ whereas the reference UA-TPDA-APAF presented a slight increase of CH₄ permeability with pressure. It is apparent that the CH₄ permeability of PIM-6FDA-OH steadily increased with increasing CO₂ fugacity, from 5.3 Barrer (1 bar) to 6.22 Barrer (15 bar) and 7.87 Barrer (21 bar). The resistance to plasticization of PIM-6FDA-OH diminished, especially in the vicinity of CO₂ fugacity at 15 bar and 21 bar.

It has been suggested that highly permeable polymers are vulnerable to plasticization resistances because of large interchain spacing.^{38,39} Obviously, the most permeable **CoPI-TB-6** membrane presented a plasticization response near a CO₂ fugacity of 10 bar. The intrachain rigidity is insufficient to thoroughly inhibit CO₂-induced plasticization.^{38,40} However, it is desirable for polymer membranes to resist plasticization through an optimal balance between interchain rigidity (*e.g.*, *via* dipole-dipole interactions, hydrogen-bonding, CTCs) and interchain spacing.⁴⁰ Two phthalimides from **An-BPDA** moieties in the backbone with similarly-planar strips (Fig. 1(b)) should facilitate co-planarization with a low rotation energy barrier between the adjacent *N*-phenyl imide groups to form interchain CTCs, thus inhibiting plasticization.^{38,40} Although increasing the fluorene-based TB units in the backbone could significantly enhance the intrachain rigidity (Fig. 1(c)), the concentration of **An-BPDA** moieties would decrease accordingly, decreasing the interchain CTC interactions. Moreover, the interchain spacing will increase with an increase in the fluorene-based TB units. These two factors are most likely responsible for the obvious plasticization phenomenon of the most permeable **CoPI-TB-6**. However, the copolymerization of two structural compositions with the appropriate units combines desirable interchain interactions, high intrachain rigidity, and interchain spacing, effectively inhibiting plasticization for the moderately permeable **CoPI-TB-x** ($x = 1-5$) membranes.

5.15. A preliminary study on changes in the gas separation performance with exposure to atmospheric water and CO₂ and aging

To evaluate the influence of exposure to atmospheric water and carbon dioxide on the change of gas separation behaviors for CoPI-TB membranes, a preliminary single gas permeability test was investigated with **CoPI-TB-1** and **CoPI-TB-2** membranes. Each membrane was prepared following the previous membrane fabrication method (Section S3, ESI[†]). First, permeation measurements were conducted on the as-cast membranes. After the first measurements, each membrane was exposed to the ambient room environment of 22 °C and 24% RH for seven days. After seven days, the second permeation measurements were conducted as before. The permeation data is tabulated in Table S6 and compared to that of PIM-based TB polymers.

As listed in Table S6, the single gas permeabilities for FDA-based **CoPI-TB-1** and **CoPI-TB-2** membranes were retained or slightly decreased during the seven day exposure to ambient atmospheric water and CO₂. Note that the decrements, if any, were quite negligible. The decrements in the permeability for **CoPI-TB-1** membranes were almost zero for N₂, O₂, CH₄ and CO₂, and < 3% for He and H₂. Those for **CoPI-TB-2** membranes were at most 9% for CH₄. Ideal selectivities were almost the same or slightly increased. This trend shows a typical characteristic of physical aging phenomena (*i.e.*, loss in free volume and chain relaxation over time).^{41,42} Apart from limitations in measurement accuracy of He and H₂ using time-lag apparatus, almost all the diffusivities decreased as shown in Table S6. Note that the reduction in gas diffusivities in **CoPI-TB-2** membranes was about 15%, which is larger than that for the **CoPI-TB-1** membranes (~7%). This difference between the two membranes can be directly ascribed to the molecular packing of the corresponding polymer matrix. A greater content of

bulky fluorene units in **CoPI-TB-2** polymers inhibited efficient chain packing and imparted additional free volume. However, at the same time, it also created additional spaces to accelerate the physical aging.

This relationship between the intrinsic free volume element and the rate of physical aging can be also extended by comparing CoPI-TB membranes in this study to reported PIM-TB polymers; the first reported TB-based PIMs for membrane gas separation applications was PIM-EA-TB.²⁷ PIM-EA-TB, the most permeable TB-based PIMs, showed a dramatic loss in the gas diffusivities and a consequent reduction in gas permeabilities compared with CoPI-TB membranes. For example, the initial CO₂ permeability of PIM-EA-TB was 7140 Barrer, which decreased by 29% to 5100 Barrer during 24 h. This decrement is four times larger than the case of **CoPI-TB-2** (7% loss, 7-day-old). Apart from the microporosity derived from the TB units, the high free volume and high permeability characteristics of PIM-EA-TB originate from the three-dimensional ethanoanthracene moieties. However, in the present CoPI-TB membranes, the introduction of bulky fluorene diamines imparted free volume elements, whereas BPDA reduced free volume elements. As shown in Table S6, the CO₂ diffusivity for **CoPI-TB-2** (57×10^9 cm²/sec) was 15 times smaller than PIM-EA-TB (870×10^9 cm²/sec). Therefore, CoPI-TB membranes in this study showed negligible deterioration in gas separation performances after 7 days exposure to atmospheric water and CO₂ and an endurance to physical aging responses compared with other PIM-TBs.

Table S6. Single gas permeability (*P*), diffusivity (*D*), solubility (*S*), and ideal selectivity (α)^b for CoPI-TB-1 and CoPI-TB-2 membranes and reference polymer membranes as a comparison. Values for membrane exposed to ambient atmospheric CO₂ and water (aged for 7 days, under the relative humidity of 23~27% and the temperature 22~24 °C) are given in parentheses, ().

sample ^a		permeability (Barrer)							ideal selectivity (α) ^b			
		He ^c	H ₂ ^c	N ₂	O ₂	CH ₄	CO ₂	H ₂ /N ₂	H ₂ /CH ₄	H ₂ /CO ₂	CO ₂ /CH ₄	CO ₂ /N ₂
CoPI-TB-1	<i>P</i>	110 (107)	202 (196)	6 (6)	26 (26)	5 (5)	110 (109)	33 (35)	37 (39)	1.8 (1.8)	20 (21)	18 (20)
	<i>D</i>	3931 (6562)	3253 (3793)	37 (29)	113 (112)	7.6 (7.1)	41 (39)	88 (130)	429 (536)	79 (98)	5.4 (5.5)	1.1 (1.3)
	<i>S</i>	0.21 (0.1)	0.5 (0.4)	1.3 (1.4)	1.8 (1.7)	5.5 (5.5)	20 (21)	0.37 (0.27)	0.09 (0.07)	0.02 (0.02)	3.7 (3.6)	16 (15)
CoPI-TB-2	<i>P</i>	155 (156)	291 (283)	8.1 (7.4)	38 (35)	7.6 (6.9)	154 (143)	36 (38)	39 (41)	1.9 (2.0)	20 (21)	19 (19)
	<i>D</i>	7183 (19405)	4415 (6200)	40 (41)	160 (136)	10 (8.4)	57 (49)	111 (152)	441 (742)	78 (125)	5.7 (5.9)	1.4 (1.2)
	<i>S</i>	0.16 (0.06)	0.5 (0.3)	1.6 (1.4)	1.8 (2.0)	5.7 (6.3)	21 (22)	0.31 (0.25)	0.09 (0.06)	0.02 (0.02)	3.6 (3.5)	13 (16)
PIM-EA-TB ^{d 27}	<i>P</i>	2570 (2720)	7760 (7310)	525 (380)	2150 (1630)	699 (572)	7140 (5100)	15 (19)	11 (13)	1.1 (1.4)	10 (8.9)	14 (13)
	<i>D</i>	>100000 (>6000)	>70000 (>50000)	1000 (410)	3180 (1770)	360 (120)	870 (410)	90 (>122)	>194 (>417)	>80 (>122)	2.4 (3.4)	1.0 (1.0)
	<i>S</i>	<0.2 (<0.3)	<0.8 (<1.1)	4.7 (7.0)	6.0 (6.9)	15 (36)	57 (92)	<0.06 (<0.16)	<0.05 (<0.03)	<0.01 (<0.01)	3.8 (2.6)	12 (13)
PIM-SBI-TB ^{d 27}	<i>P</i>	878 (858)	2200 (2110)	232 (215)	720 (657)	450 (406)	2900 (2720)	9.4 (9.8)	4.9 (5.2)	0.8 (0.8)	6.4 (6.7)	13 (13)
	<i>D</i>	>50000 (>50000)	>35000 (>30000)	750 (700)	2010 (1870)	320 (190)	740 (660)	45 (>43)	>109 (>158)	>47 (>45)	2.3 (3.5)	1.0 (1.0)
	<i>S</i>	<0.12 (<0.12)	0.47 (<0.5)	2.3 (2.3)	2.7 (2.6)	11 (11)	30 (31)	<0.20 (<0.22)	0.04 (<0.05)	0.02 (<0.02)	2.7 (2.8)	13 (13)

^a Units: *P*: 10⁻¹⁰cm³(STP)/cm sec cmHg, *D*:10⁻⁹cm²/sec, and *S*: cm³(STP)/cm³ atm, measured at 3 bar, 35 °C;

^b Ideal selectivity $\alpha=P_1/P_2$;

^c Data for He and H₂ from the time-lag apparatus result in significant experimental errors in determining the diffusivity and solubility due to very short lag-times^{3, 27};

^d measured at 1 bar, 25 °C. Aged for just one day.

Notes and references

1. C.-H. Chou, D. S. Reddy and C.-F. Shu, *J. Polym. Sci. Part A: Polym. Chem.*, 2002, **40**, 3615-3621.
2. Y. Zhuang, J. G. Seong, Y. S. Do, H. J. Jo, Z. Cui, J. Lee, Y. M. Lee and M. D. Guiver, *Macromolecules*, 2014, **47**, 3254-3262.
3. J. G. Seong, Y. Zhuang, S. Kim, Y. S. Do, W. H. Lee, M. D. Guiver and Y. M. Lee, *J. Membr. Sci.*, 2015, **480**, 104-114.
4. Y. Zhuang, J. G. Seong, Y. S. Do, W. H. Lee, M. J. Lee, M. D. Guiver and Y. M. Lee, *J. Membr. Sci.*, 2016, **504**, 55-65..
5. M. Calle, C. M. Doherty, A. J. Hill and Y. M. Lee, *Macromolecules*, 2013, **46**, 8179-8189.
6. N. Du, J. Song, G. P. Robertson, I. Pinnau and M. D. Guiver, *Macromol. Rapid Commun.*, 2008, **29**, 783-788.
7. M. Carta, M. Croad, R. Malpass-Evans, J. C. Jansen, P. Bernardo, G. Clarizia, K. Friess, M. Lanč and N. B. McKeown, *Adv. Mater.*, 2014, **26**, 3526-3531.
8. R. Swaidan, M. Al-Saedi, B. Ghanem, E. Litwiller and I. Pinnau, *Macromolecules*, 2014, **47**, 5104-5114.
9. H. Wang, D. R. Paul and T. S. Chung, *J. Membr. Sci.*, 2013, **430**, 223-233.
10. H.-Y. Zhao, Y.-M. Cao, X.-L. Ding, M.-Q. Zhou, J.-H. Liu and Q. Yuan, *J. Membr. Sci.*, 2008, **320**, 179-184.
11. S. S. Hosseini, M. M. Teoh and T. S. Chung, *Polymer*, 2008, **49**, 1594-1603.
12. W.-H. Lin and T.-S. Chung, *J. Membr. Sci.*, 2001, **186**, 183-193.
13. X. H. Ma, R. Swaidan, Y. Belmabkhout, Y. H. Zhu, E. Litwiller, M. Jouiad, I. Pinnau and Y. Han, *Macromolecules*, 2012, **45**, 3841-3849.
14. X. H. Ma, O. Salinas, E. Litwiller and I. Pinnau, *Macromolecules*, 2013, **46**, 9618-9624.
15. X. Ma, B. Ghanem, O. Salinas, E. Litwiller and I. Pinnau, *ACS Macro Letters*, 2015, **4**, 231-235.
16. Y. J. Cho and H. B. Park, *Macromol. Rapid Commun.*, 2011, **32**, 579-586.
17. B. S. Ghanem, N. B. McKeown, P. M. Budd, N. M. Al-Harbi, D. Fritsch, K. Heinrich, L. Starannikova, A. Tokarev and Y. Yampolskii, *Macromolecules*, 2009, **42**, 7881-7888.
18. Y. Rogan, L. Starannikova, V. Ryzhikh, Y. Yampolskii, P. Bernardo, F. Bazzarelli, J. C. Jansen and N. B. McKeown, *Polym. Chem.*, 2013, **4**, 3813-3820.
19. Y. Rogan, R. Malpass-Evans, M. Carta, M. Lee, J. C. Jansen, P. Bernardo, G. Clarizia, E. Tocci, K. Friess, M. Lanc and N. B. McKeown, *J. Mater. Chem. A*, 2014, **2**, 4874-4877.
20. S. Kazama, T. Teramoto and K. Haraya, *J. Membr. Sci.*, 2002, **207**, 91-104.
21. K. Tanaka, H. Kita, K. Okamoto, A. Nakamura and Y. Kusuki, *J. Membr. Sci.*, 1989, **47**, 203-215.
22. Y. Hirayama, T. Yoshinaga, Y. Kusuki, K. Ninomiya, T. Sakakibara and T. Tamari, *J. Membr. Sci.*, 1996, **111**, 169-182.
23. F. Piroux, E. Espuche, R. Mercier, M. Pinéri and G. Gebel, *J. Membr. Sci.*, 2002, **209**, 241-253.
24. C. A. Scholes, C. P. Ribeiro, S. E. Kentish and B. D. Freeman, *J. Membr. Sci.*, 2014, **450**, 72-80.
25. B.-W. Chun, C. Ishizu, H. Itatani, K. Haraya and Y. Shindo, *J. Poly. Sci., Part B: Polym. Phys.*, 1994, **32**, 1009-1016.
26. S. Kim and Y. M. Lee, *Prog. Polym. Sci.*, 2015, **43**, 1-32.
27. M. Carta, R. Malpass-Evans, M. Croad, Y. Rogan, J. C. Jansen, P. Bernardo, F. Bazzarelli and N. B. McKeown, *Science*, 2013, **339**, 303-307.
28. S. Kim, J. G. Seong, Y. S. Do and Y. M. Lee, *J. Membr. Sci.*, 2015, **474**, 122-131.
29. O. C. David, D. Gorri, A. Urtiaga and I. Ortiz, *J. Membr. Sci.*, 2011, **378**, 359-368.
30. L. Shao, C.-H. Lau and T.-S. Chung, *Int. J. Hydrogen Energy*, 2009, **34**, 8716-8722.
31. S. Park, A. S. Lee, Y. S. Do, S. S. Hwang, Y. M. Lee, J.-H. Lee and J. S. Lee, *Chem. Commun.*, 2015, **51**, 15308-15311.
32. F. de Clippel, A. L. Khan, A. Cano-Odena, M. Dusselier, K. Vanherck, L. Peng, S. Oswald, L. Giebeler, S. Corthals, B. Kenens, J. F. M. Denayer, P. A. Jacobs, I. F. J. Vankelecom and B. F. Sels, *J. Mater. Chem. A*, 2013, **1**, 945-953.
33. V. Bondar, A. Alentiev, T. Masuda and Y. Yampolskii, *Macromol. Chem. Phys.*, 1997, **198**, 1701-1708.
34. C. H. Lau, P. Li, F. Li, T.-S. Chung and D. R. Paul, *Prog. Polym. Sci.*, 2013, **38**, 740-766.
35. T. Visser, N. Masetto and M. Wessling, *J. Membr. Sci.*, 2007, **306**, 16-28.
36. R. Swaidan, B. Ghanem, E. Litwiller and I. Pinnau, *J. Membr. Sci.*, 2015, **475**, 571-581.
37. M. Calle, H. J. Jo, C. M. Doherty, A. J. Hill and Y. M. Lee, *Macromolecules*, 2015, **48**, 2603-2613.
38. R. Swaidan, B. Ghanem, E. Litwiller and I. Pinnau, *Macromolecules*, 2015, **48**, 6553-6561.
39. W. J. Koros and D. R. B. Walker, *Polym J*, 1991, **23**, 481-490.
40. R. Swaidan, B. Ghanem, M. Al-Saedi, E. Litwiller and I. Pinnau, *Macromolecules*, 2014, **47**, 7453-7462.
41. Y. Huang and D. R. Paul, *Polymer*, 2004, **45**, 8377-8393.
42. M. S. McCaig and D. R. Paul, *Polymer*, 2000, **41**, 629-637.